Ion-Beam-Induced Bending of Semiconductor Nanowires

Imran Hanif [a*]***, Osmane Camara***[a]***, Matheus A. Tunes***[a]***, Robert W. Harrison***[a]***, Graeme Greaves***[a]***, Stephen E. Donnelly***[a] ***and Jonathan A. Hinks***[a]

[a]*School of Computing and Engineering, University of Huddersfield, Queensgate, Huddersfield, HD1 3DH, United Kingdom*

[*]*Corresponding Author:* imran.hanif@alumni.hud.ac.uk

Abstract

The miniaturization of technology increasingly requires the development of both new structures as well as novel techniques for their manufacture and modification. Semiconductor nanowires (NWs) are a prime example of this and as such have been the subject of intense scientific research for applications ranging from microelectronics to nano-electromechanical devices. Ion irradiation has long been a key processing step for semiconductors and the natural extension of this technique to the modification of semiconductor NWs has led to the discovery of ion-beam-induced deformation effects. In this work, transmission electron microscopy with *in-situ* ion bombardment has been used to directly observe the evolution of individual silicon and germanium NWs under irradiation. Silicon NWs were irradiated with either 6 keV neon ions or xenon ions at 5, 7 or 9.5 keV with a flux of 3×10^{13} ions/cm^2/s. Germanium NWs were irradiated with 30 or 70 keV xenon ions with a flux of 10^{13} ions/cm^2/s. These new results are combined with those reported in the literature in a systematic analysis using a custom implementation of the *Transport of Ions in Matter* Monte Carlo computer code to facilitate a direct comparison with experimental results taking into account the wide range of experimental conditions. Across the various studies this has revealed underlying trends and forms the basis of a critical review of the various mechanisms which have been proposed to explain the deformation of semiconductor NWs under ion irradiation.

1. Introduction

Semiconductor nanowires (NWs) are leading candidates for use in future generations of nanotechnologies as components including resonators [1], diodes [2,3], transistors [4–7], generators [8] and sensors [9–12]. As well as their nanoscale lateral dimensions, their properties and behaviour are also made distinct from their bulk counterparts by virtue of their large surface-to-volume ratios [2,10], [13–15], quantum effects [2,5,14] and degrees of physical freedom which allow increased possibilities for deformation and assembly [16]. Ion or electron irradiation can cause self-assembly, local chemical reactions, doping or sputtering to enable tailoring of nanostructures [17].

Ion beams have been used to modify semiconductors since the 1950s [18–20] to control properties including electrical [21,22], optical [22–25], mechanical [21,26], thermal [27] and surface morphology [23,28]. Such methods can be similarly applied to the tailoring of these characteristics in semiconductor NWs [1,4,13,29,30]. Additionally, ion beam techniques can be applied to NWs in order to engineer their shape and alignment [31], in their synthesis [32–35] and in their machining [36].

Whilst the consequences of ion irradiation are well understood in bulk semiconductors [21,22,27,37], investigations are required to understand the differences in the NWs case and thus develop the tools required for modification of their properties (structural, mechanical and electronic) and incorporation into nanoscale devices for achieving desired functions and applications such as nanowire-based field effect transistors [38]. The effects of ion beams can be both desirable and deleterious, depending on the application, with effects including the sputtering of material [39,40], implantation of intrinsic and extrinsic atoms [41–45] and crystallographic damage ranging from point defects [29,46–49] to complete amorphization [50–57].

One particular ion-irradiation-induced phenomenon which has been the subject of intense research in recent years is the bending of semiconductor NWs [58–64]. This has been observed in silicon [16,60–62], germanium [63], gallium arsenide [58] and zinc oxide [59] NWs with various explanations for the underlying mechanisms for this behaviour presented in the literature

[58, 60, 62-65]. In gallium arsenide [58] and zinc oxide [59] NWs, Borschel *et al.* have used various combinations of ion species and energies to achieve different damage distributions as functions of depth (hereafter, referred to as "damage profiles" for brevity).

They found that shallow damage profiles caused bending away from the ion beam direction and deeper profiles caused bending towards it with both conditions causing deformation starting from low sub-amorphization-threshold fluences. Using a custom implementation of the *Transport of Ions in Matter* (TRIM) code adapted to perform calculations for three-dimensional structures [66], they concluded that the direction of bending was determined by the relative concentrations of vacancies and interstitials across the NW. At their highest damage levels, sputtering and the resulting thinning of the NWs was also suggested to be a factor.

Pecora *et al.* have reported on the ion-beam-induced bending of tapered silicon NWs (radius = 49±16 nm at base) under Ge ion irradiation at 45 keV and 70 keV [60,61]. They observed that bending towards the ion beam direction occurred but only above a critical fluence corresponding to the threshold for complete amorphization and, at the highest fluences, NWs which had previously been angled away from the ion beam became parallel to it (see figure S1 and video clip S2 in the Supplementary Material for illustrative examples from the current work of nanowires undergoing similar transformations). This requirement for complete amorphization prior to bending towards the ion beam has also been observed by Romano *et al*. [63]. In their work, germanium NWs of diameter ~50 nm were irradiated using 30 keV gallium ions in a focused ion beam (FIB) system. With the beam initially incident at 45° to the axis of the NWs, using *in-situ* scanning electron microscopy (SEM) they were seen to bend towards the ion beam and the deformation could be repeatedly reversed by irradiating from the opposite direction. Even above damage levels expected to induce complete amorphization, the NW continued to demonstrate a bending response to irradiation. Due to the observed necessity for amorphization before bending both Pecora *et al*. and Romano *et al.* attributed the mechanism to a model of viscoelastic flow proposed by Trinkaus *et al.* [67] which requires amorphous material. In this model, electronic energy losses cause anisotropic heating of a

cylindrical volume along the ion track resulting in expansion and shear stress. Upon relaxation this causes expansion perpendicular to, and contraction parallel to, the ion track in a constant-volume anisotropic plastic deformation. Although Romano *et al*. did not come to a firm conclusion regarding the process driving the bending, they suggested that a densification may be induced by the irradiation without speculating as to the exact mechanism. Pecora *et al.* also found that under irradiation conditions which did not amorphize the entire width of a NW, the remaining strip of crystalline material could inhibit bending. Furthermore, under annealing, the NWs could be straightened in the presence of a crystalline-amorphous interface to facilitate solid-phase epitaxial growth (SPEG) or the NW could remain bent if the recrystallization progressed by randomly-nucleated growth (RNG).

Three-dimensional patterning of silicon NWs has been demonstrated by Jun *et al.* [16] by varying the incident direction of 30 keV gallium ion irradiation in a FIB system to create shapes such as hooks or springs. At low doses, bending was found to be away from the ion beam and at higher doses towards the ion beam. They further demonstrated the wider occurrence of the phenomenon through extension to oxidised silicon, gallium nitride and zinc oxide NWs.

Rajput *et al.* [62] have reported the bending of polycrystalline silicon NWs irradiated at 36° to the axis of the NWs with 16 keV gallium ions in a FIB system. The NWs were observed to bend towards the ion beam upon irradiation until they aligned parallel to the ion beam direction. They reported that ion beam induced sputtering and dynamic annealing of defects caused a significant amount of compressive stresses on the irradiated side of the NW. They concluded that ion-beam-induced compressive stresses on the irradiated side of the NW shrinks the surface and causes a deformation in the system resulting in the NW bending towards the ion beam.

Cui *et al.* [65] have investigated the effects of substrate conductivity on the bending of metal NWs. Amorphous tungsten NWs were grown on three different substrates of Si/SiO_2, $Au/SiO_2/Si$ or aluminium and platinum NWs were grown on aluminium substrates. They used a raster scan to irradiate the NWs using 30 keV gallium ions in a FIB system. They observed that the amorphous

tungsten NWs grown on Si/SiO_2 and $Au/SiO_2/Si$ substrates first bent away and then towards the ion beam while the amorphous tungsten and platinum NWs grown on aluminium substrates bent towards the ion beam direction. The authors did not conclude a definite mechanism of bending but suggested that electrical conductivity of the substrate and variation of beam current and scan time during the ion beam raster may play a role in NW bending.

This paper presents new results on the bending of silicon and germanium NWs induced by ion irradiation performed *in-situ* whilst under observation in a transmission electron microscope (TEM[1]). These results are combined with those from the literature and subjected to a systematic analysis to allow direct comparison taking into account the different irradiation conditions, experimental techniques and the NW properties. This approach has allowed key similarities and differences to be highlighted with universal trends revealed to give greater insight into the driving mechanisms behind the bending.

2 Experimental Methods

Polydispersed silicon NWs (purity > 99%) with typical diameters of 50 nm and lengths of 1–20 μm were obtained from Sigma-Aldrich (product number 731498) in powder form and were suspended in ethanol by agitating in an ultrasonic bath at room temperature for 90 minutes. Single-crystal germanium NWs (purity > 99%) grown on silicon wafers using chemical vapour deposition were obtained from Nanowires Tech Limited (product number GNWsl15). The germanium NWs were separated from the silicon wafer using an ultrasonic bath of ethanol at room temperature for 15 minutes. In both cases, the resulting solution was drop cast by syringe onto 400-mesh molybdenum TEM grids at room temperature and the ethanol was allowed to evaporate leaving the NWs deposited on the grids.

TEM with *in-situ* ion irradiation experiments were performed at room temperature in the Microscopes and Ion Accelerators for Materials Investigations (MIAMI-1) facility at the University

[1] In this paper, the abbreviation TEM is used to refer to both the instrument (transmission electron microscope) and the technique (transmission electron microscopy).

of Huddersfield which is described in detail elsewhere [68]. This technique allows an individual nanowire to be followed throughout the irradiation (see video clip S2 in the Supplementary Material); not only does this allow the dynamic behaviour to be captured but it also ensures that the same nanostructure is being studied both before and after irradiation (a particular concern in experiments designed to induced significant morphological changes). Furthermore, it allows accurate determination of the angle of incidence of the ion beam relative to the axis of the nanowire as described below. The geometry of the sample, electron beam and ion irradiation are illustrated schematically in Figure 1. The JEOL JEM-2000FX TEM in the MIAMI-1 facility was operated at 100 kV and the electron beam was kept on during ion irradiation in order to facilitate *in-situ* observation. Experiments with the electron beam off during ion irradiation to check for any possible electron beam effects yielded similar results to those presented here with the electron beam on. Samples were loaded into a JEOL EM-BSR tilt-rotate holder which enables a NW of interest to be manipulated into the desired orientation relative to the ion beam. This holder also allowed pre- and post-irradiation tilt series to be performed to detect curvature and inclination as described below. For each experiment, a single-crystal NW was selected which was found to be attached to the grid at one end with the other end suspended in free space.

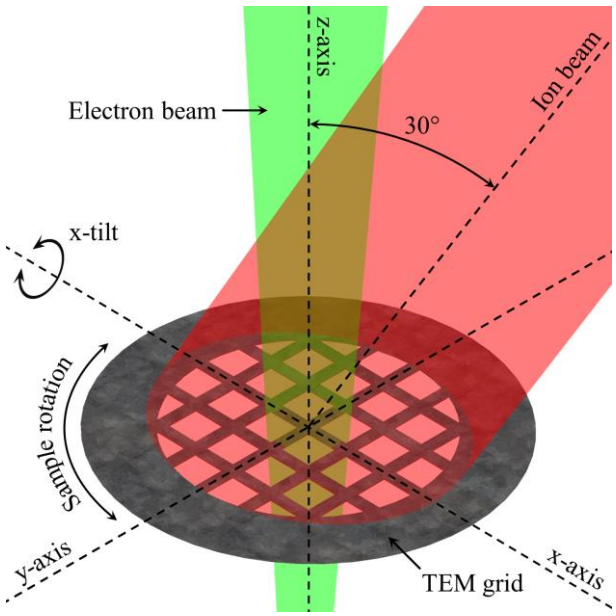

Figure 1: *Schematic of the geometry of the sample, electron beam and ion irradiation in the MIAMI-1 facility. Rotation about the x-axis allows the tilt series illustrated in figure 2 to be captured and rotation about the z-axis allows ion irradiation normal to axis of a NW to be performed.*

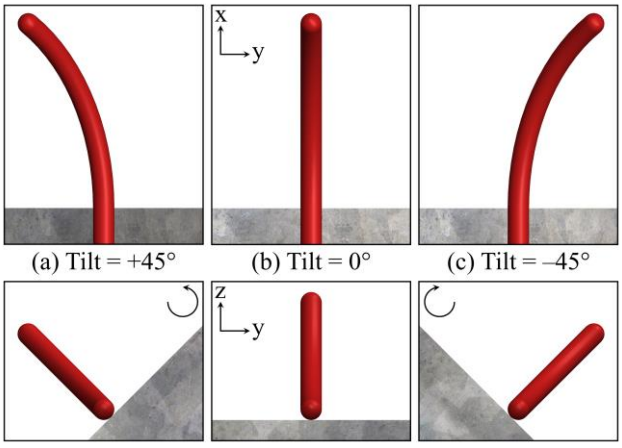

Figure 2: *A series of schematics showing a NW (red) on a TEM grid (grey) and the tilt series methodology used to determine the bending direction due to in-situ ion irradiation within a TEM at the MIAMI-1 facility. The top row shows the view along the z-axis (i.e. the electron beam direction and thus what is observed in projection) of the TEM demonstrating how the curvature of a NW can be hidden or revealed depending on the angle of goniometer x-tilt. The bottom row shows the view along the x-axis*

demonstrating that the top row corresponds to a NW bending upwards in the TEM. If the bending direction of the NW were reversed (i.e. pointing downwards in the TEM) then the projected views down the z-axis would also be reversed. Similarly, this technique can be used to detect the inclination of a NW (i.e. its deflection out of the xy-plane of the TEM) prior to selection for an irradiation experiment.

The curvatures of the NWs were evaluated as illustrated in Figure 2. Each NW was rotated such that it became aligned along the x-axis of the TEM. Images were then captured at x-tilt angles of –45°, 0° and +45° allowing the direction of any curvature and inclination to be measured. This was vital in order to accurately determine the angle of incidence of the ion beam which can significantly alter the lateral range of ions in a target. The NW was then returned to 0° tilt and rotated such that its axis became perpendicular to the direction of the ion beam in the geometry of the MIAMI-1 facility. The silicon NWs were irradiated and the images were again captured at x-tilts of –45°, 0° and +45°. Silicon NWs were irradiated with either 6 keV neon ions or xenon ions at 5, 7 or 9.5 keV with a flux on the order of 3×10^{13} ions/cm^2/s. Germanium NWs were irradiated with 30 or 70 keV xenon ions with a flux of 10^{13} ions/cm^2/s.

2.1 Calculation Methods

The *Transport of Ions in Matter* (TRIM) Monte Carlo computer code is freely available and widely used to calculate ion-irradiation damage and implantation profiles [69]. However, the code in its native form is limited to planar targets which do not reflect the cylindrical geometry of a NW. Several approaches have been taken attempting to address this issue including the Iradina [64], 3dTRIM [70], TRI3DYN [71] and IM3D [72] computer codes. Of these, only Iradina is open source and freely available but is optimised for speed through the use of look-up functions taken from the Corteo program [73]. In order to allow the analysis reported here to be reproduced by others, to utilise the full Monte Carlo capabilities of TRIM and to facilitate the large number of calculations

required to complete the literature survey, TRIM was run in the batch mode using an open-source MATLAB code called *Ion Damage and RAnge in the Geometry Of Nanowires* (IDRAGON). The IDRAGON simply imports results from TRIM into MATLAB to build the NW profiles under different irradiation conditions using a multislice approach. A publication is in preparation which will detail the workings of the IDRAGON source code which will also be available to download. The IDRAGON code runs TRIM for various target depths corresponding to the equally-spaced parallel-chords of a circle which are combined into a multislice model. The two-dimensional atomic displacement and implantation profiles created in this way are then used to generate colour-scale plots across the cross-section of the NWs as shown in Figure 3.

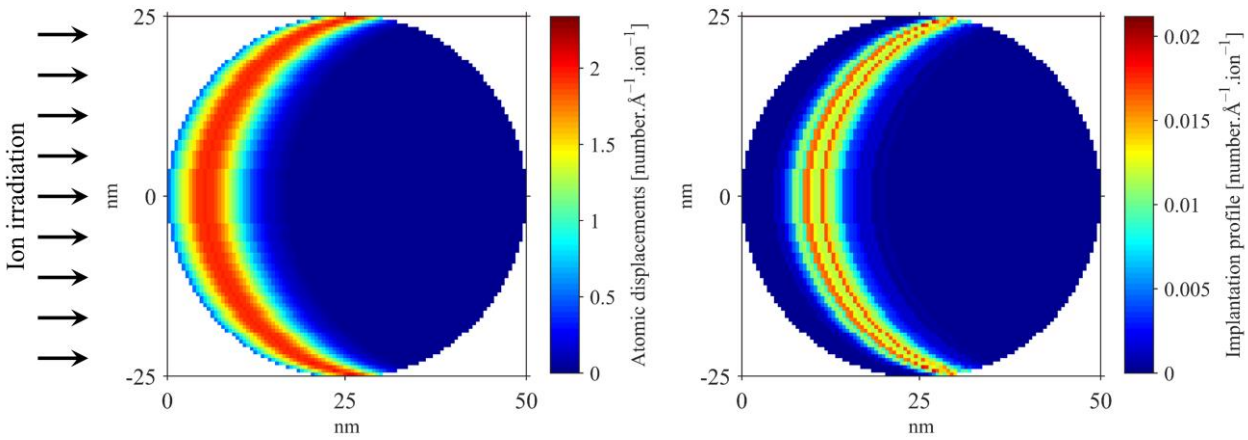

Figure 3: *Example of a TRIM multislice calculation of the distributions of: (a) atomic displacements; and (b) ion implantation for 7 keV xenon ions incident on a silicon NW of diameter 50 nm.*

The TRIM calculations within the IDRAGON code were performed using version 2013 run in the "Detailed calculation with full damage cascades" mode for 1000 ions per slice using the material properties given in table 1 and the irradiation parameters detailed in table 2. The lattice and surface energies were both set to 0 eV [74]. The number of atomic displacements was found by summing the number of vacancies and of replacement collisions. The average depths of the atomic displacements ($\bar{x}_{\mathrm{disp}}$) and implanted ions ($\bar{x}_{\mathrm{ion}}$) were determined using Equation 1:

$$\bar{x} = \frac{\sum_{n=1}^{100}\left(\frac{\sum_{m=1}^{100}\left(N_{m,n} \times x_m\right)}{\sum_{m=1}^{100} N_{m,n}}\right)}{100} \qquad \text{Equation 1}$$

Where $\bar{x}$ is $\bar{x}_{\text{disp}}$ (or $\bar{x}_{\text{ion}}$) and $N_{m,n}$ is the number of atomic displacements (or implanted ions) calculated by TRIM in slice n at depth x_m in the multislice model. Zero depth was taken as zero on the x-axis of the plots shown (rather than being at the surface of the NW) such that a depth of $x = 0.5$ corresponds to the central line through the cross section of a NW.

Table 1: *Material properties used as inputs for TRIM calculations.*

Material	**Density (g.cm^{-3})**	**E_d (eV)**	**Reference**
Gallium arsenide	5.32	Gallium = 15 Arsenic = 15	[75]
Germanium	5.32	21	[76]
Silicon	2.33	20	[77]
Zinc oxide	5.51	Zinc = 65 Oxygen = 50	[78]

The approach taken by the IDRAGON code does not allow communication between the slices and so the lateral ranges of the incident ions and knock-on atoms which would take them out of their slice of origin are not taken into account. However, as neighbouring slices are of very similar lengths, approximately the same number would enter each slice as would escape. This becomes more significant in slices nearer the edge of the circular cross-section as the possibility of an incident ion or knock-on atom exiting the NW (other than at the end of the slice) is not considered. Therefore, the damage and implantation in the outermost slices are likely to be slightly overestimated and as these slices are those in which the profiles are deepest (in terms of x as defined above for Equation 1) then $\bar{x}$ is also likely to be slightly overestimated by IDRAGON.

3 Results and Discussions

3.1 Analysis of current results and literature survey

The experimental parameters and results presented here and reported in the literature have been collated in order to allow a systematic analysis to identify universal trends in the bending behaviour and the ion irradiation conditions. Using the IDRAGON code, damage and implantation profiles were calculated which allow direct comparison.

The threshold fluences for the amorphization of silicon by 6 keV neon ions have been calculated to be 1.9×10^{15} ions/cm^2 to a depth of 19 nm and by 5, 7 or 9.5 keV xenon ions to be 1.1×10^{15}, 7.7×10^{14} and 5.8×10^{14} ions/cm^2 to depths of 9, 11 and 14 nm, respectively, based on an amorphization threshold of 0.9 DPA for neon [79] and 0.5 DPA for xenon [80] irradiation in this energy regime. In these experiments, silicon NWs were irradiated with neon to an end fluence of 2.16×10^{16} ions/cm^2 or with xenon ions to end fluences of between 3.5×10^{15} and 2.2×10^{16} ions/cm^2. The threshold fluences for the amorphization of germanium by 30 or 70 keV xenon have been calculated to be 9.4×10^{13} and 4.2×10^{13} ions/cm^2 to depths of 20 and 34 nm, respectively, based on an amorphization threshold of 0.3 DPA [81] in this energy regime. In the experiments reported here, the germanium NWs were irradiated with xenon ions to end fluences of between 2.8×10^{13} and 4.7×10^{14} ions/cm^2. Therefore, based on the values in the literature for bulk silicon and germanium it is expected that many of the NWs would have developed amorphous layers by the end of the irradiations in the experiments reported here. However, bending was observed to occur immediately upon exposure to the ion beam in the current work. For example, video clip S2 in the Supplementary Material shows a silicon nanowire (at four times real speed) whilst under irradiation with 7 keV Xe ions at a flux of 1.2×10^{14} ions/cm^2/s (giving an effective flux in the video clip of 4.8×10^{14} ions/cm^2/s); the irradiation and the video clip start at the same time and it can be seen that the bending is immediate and that a significant amount occurs in the first fractions of a second in

which time only a relatively small proportion of the threshold amorphization fluence would have been accumulated.

Table 2 presents the results of the survey and the calculations with the experiments grouped by material and sorted by the normalised average damage depth, $\bar{x}_{\mathrm{disp}} / Ø$, where $Ø$ is a diameter of the NW. As can be seen, for each semiconductor material there is a correlation between the damage depth and the bending behaviour; the bending is away from the ion beam for shallower damage and the bending is towards for deeper profiles. The ranges of damage and implantation depth in which this reversal occurs for each material are summarised in table 3. The correlation of bending direction with implantation depth is also consistent with the slight exception of the silicon case for which the conditions for bending away or towards the ion beam demonstrate a small degree of overlap.

This correlation of damage depth with bending direction has been identified by previous authors including Borschel *et al.* [58,59]. However, what is notable for all the semiconductor NW materials irradiated for the current work and reported in the literature is that the reversal of the bending occurs for average damage depths well within the half of the NW nearest the irradiated surface (i.e. $\bar{x}_{\mathrm{disp}} / Ø < 0.5$). As discussed above, the IDRAGON code will have a tendency to overestimate the average depths of the damage and implantation profiles meaning that the reversal points are likely even shallower than suggested by the results presented in tables 2 and 3.

Bending mechanisms which are driven by atomic displacements within the NW, such as the accumulation of point defects, will cause expansion as interstitials induce more swelling than vacancies induce contraction [49] and ultimately accumulate, either heterogeneously or homogeneously, causing a transition to the less dense (i.e. expanded) amorphous phase. Therefore, if such processes are concentrated in the first half of the NW then they will drive bending away from the ion beam. This leads to the conclusion that other mechanism(s) must be dominating in the case of $\bar{x}_{\mathrm{disp}} / Ø < 0.5$ irradiations which induce bending towards the ion beam.

Possible candidates for mechanisms which could dominate over those driven by atomic

displacements to induce bending towards the ion beam for values of $\bar{x}_{disp}$ / Ø < 0.5 include sputter-induced surface reconstruction, the relief of tensile stress at the irradiated surface and the spatial separation of the distributions of vacancies and interstitials. However, the separation of the vacancies and interstitials would also operate for the shallowest irradiations which induce bending away from the ion beam; for this reason and for the further reasons discussed in section 3.4 below, this can be ruled out as a dominant mechanism. All the other mechanisms proposed and listed in table 4 would cause bending away and thus re-enforce that favoured by damage accumulation for shallow irradiations.

Unless there are additional mechanisms which have not been conceived by the current and previous authors, it is therefore concluded that for the shallowest irradiations the competition is won by damage accumulation causing an expansion facilitated by the proximity of the surface which allows the induced stress to be relieved. However, for slightly deeper irradiations (but notably still $\bar{x}_{disp}$ / Ø < 0.5) the proximity of the surface and the possibilities for stress relief it affords are reduced allowing the cumulative effects of the mechanisms which favour bending towards the ion beam to dominate.

Table 2: *Summary of the experiments on the ion-irradiation-induced bending of semiconductor NWs reported in the literature combined with the results presented here. For each experiment, damage and implantation profiles are shown as calculated using the IDRAGON code. Experiments are grouped by nanowire material and ordered by the average displacement depth,* $\bar{x}_{disp}$*, relative to the nanowire diameter, Ø. The colour bar at the bottom of the table applies to both the damage and the implantation with the maximum value in each profile normalised to the maximum of the scale.*

Ref	Nanowire		Irradiation Conditions			IDRAGON Calculations				Bending [b]
	Material	Ø (nm)	Ion	*E* (keV)	θ [a]	$\bar{x}_{disp}$ / Ø	Damage	Implant	$\bar{x}_{ion}$ / Ø	
[58]	Gallium arsenide	150	Argon	35	35°	0.23			0.27	Away
[58]	Gallium arsenide	150	Xenon	80	35°	0.23			0.26	Away
[58]	Gallium arsenide	150	Sulphur	30	35°	0.23			0.28	Away
[58]	Gallium arsenide	150	Xenon	210	35°	0.34			0.42	Away
[58]	Gallium arsenide	150	Argon	210	35°	0.50			0.54	Towards
[58]	Gallium arsenide	150	sulphur	180	35°	0.50			0.55	Towards
This work	Germanium	46	Xenon	30	45°	0.29			0.33	Away
This work	Germanium	25	Xenon	70	60°	0.45			0.5	Towards
This work	Germanium	60	Xenon	30	40°	0.26			0.29	Away
[63]	Germanium	50	Gallium	30	45°	0.32			0.38	Towards

This work	Silicon	50	Xenon	5	35°	0.19		0.25	Away
[70]	Silicon	210 [c]	Gallium	30	0°	0.20		0.24	Away
This work	Silicon	50	Xenon	5	0°	0.21		0.26	Away
This work	Silicon	50	Xenon	7	0°	0.23		0.32	Away
This work	Silicon	50	Xenon	9.5	35°	0.23		0.31	Towards
This work	Silicon	50	Xenon	9.5	0°	0.25		0.35	Towards
[62]	Silicon [e]	50	Gallium	16	54°	0.27		0. 32	Towards
This work	Silicon	36	Xenon	7	0°	0.27		0.39	Towards
This work	Silicon	50	Neon	6	0°	0.33		0.40	Towards
This work	Silicon	24	Xenon	7	0°	0.35		0.53	Towards
[59]	Zinc oxide	60	Argon	20	38° [d]	0.27		0.31	Away

[59]	Zinc oxide	90	Argon	90	38° [d]	0.44			0.53	Towards

[a] Defined as the angle from the normal to the nanowire axis.
[b] Relative to the direction of the incident ion beam.
[c] Based on figure 5 and text in [70].
[d] Based on figures 1, 2 and 6 in [59].
[e] Polycrystalline silicon.

Table 3: *Normalised average damage and implantation depth correlating with the reversal of the ion-irradiation-induced bending direction for various semiconductor nanowires irradiated as part of the current work and reported in the literature.*

Nanowire	Damage Depth	Implantation Depth
Gallium arsenide	$0.34 < (\bar{x}_{disp} / Ø) < 0.50$	$0.42 < (\bar{x}_{ion} / Ø) < 0.54$
Germanium	$0.29 < (\bar{x}_{disp} / Ø) < 0.32$	$0.33 < (\bar{x}_{ion} / Ø) < 0.38$
Silicon	$0.23 < (\bar{x}_{disp} / Ø) < 0.25$	$0.26 < (\bar{x}_{ion} / Ø) < 0.35$
Zinc oxide	$0.27 < (\bar{x}_{disp} / Ø) < 0.44$	$0.31 < (\bar{x}_{ion} / Ø) < 0.53$

Table 4: *Summary of bending mechanisms and their variants including those previously proposed in the literature [58,59,61–63] and the expected bending behaviour which they would favour in the case of a shallow irradiation (i.e.* $\bar{x}_{disp} / Ø < 0.5$ *and* $\bar{x}_{ion} / Ø < 0.5$*) typical of the vast majority of experimental results summarised in table 2.*

	Mechanism	**Bending [a]**
Atomic Displacements	Accumulation of damage	Away
	Vacancy and interstitial distributions [58,59]	Towards
	Amorphization [63]	Away
Surface Effects	Sputtering induced surface reconstruction [62]	Towards
	Compressive stress relief at irradiated surface [62]	Towards
	Tensile stress relief at irradiated surface	Away
Implantation	Introduction of additional atoms	Away
Viscoelastic Flow	In thermal spike of ion track [61,63]	Towards

3.2 Density change required to induce bending

In order to explore the various mechanisms proposed to explain the bending phenomenon, it is useful to test them under maximising assumptions. If even under these modelling conditions a mechanism is unable to account for the degree of bending observed experimentally then it must be concluded that it cannot be the sole driving force for the deformation. The first maximising assumption is that the expansion and/or contraction (which we assume to be concurrent with the bending) occurs completely and exclusively in one half of the NW with the boundary between the two halves running along the arc of the induced curvature. The second maximising assumption is that there is no residual stress – i.e. all induced stress is able to relax through the bending of the NW and thus able to drive the deformation to its maximum extent.

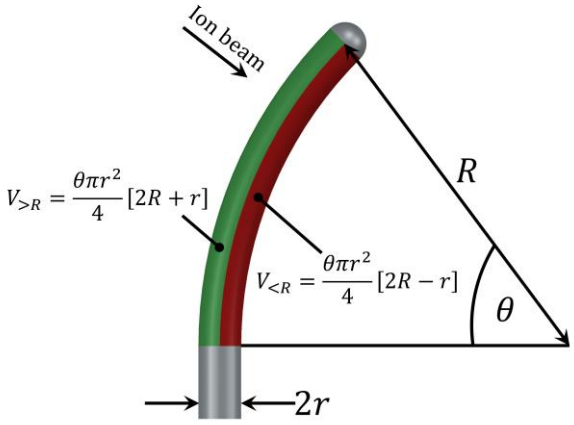

Figure 4: *Schematic of a NW of diameter,* 2*r, featuring a bent section with a radius of curvature, R,* and *arc length, θR. The volumes of the bent sections on the outside,* $V_{>R}$*, and inside,* $V_{<R}$*,* of *R are given by the expressions shown.*

Consider a bent section of a NW of diameter, $2r$, and radius of curvature, R. This can be modelled as being composed of two volumes sharing an interface running along the axis of the NW and normal to the radius of curvature as shown in Figure 4. The ratio, σ, between the volume on the outside of the radius of curvature, $V_{>R}$, and the volume on the inside, $V_{<R}$, can be calculated using

Equation 2 (see S3 in the Supplementary Material for derivation):

$$\sigma = \frac{V_{>R}}{V_{<R}} = \frac{2R+r}{2R-r} \qquad \text{Equation 2}$$

In the case of a shallow irradiation (i.e. $\bar{x}_{\text{disp}}$ / Ø < 0.5 and $\bar{x}_{\text{ion}}$ / Ø < 0.5) typical of the vast majority of experimental results summarised in table 2, it is assumed that the deformation must be accompanied by an increase in the volume of the side upon which the ions are incident (i.e. $V_{>R}$) relative to the opposite side of the NW (i.e. $V_{<R}$) and consequently the NW bends away from the ion beam as illustrated in Figure 4. This assumption is reasonable based on two experimental observations from the current work. Firstly, that bending occurred only in the plane defined by the ion beam and the axis of the NW meaning that no rotation occurred out of this plane and so the ion beam was always incident on the same area of the surface (with the exception of the very tip of the NW which would have been rotated out of the ion beam path by the bending). Secondly, apart from the bending, no other changes to the geometry or dimensions of the NWs were detected at low fluences. However, it should be noted that at much higher fluences sputtering levels were substantial enough to be observed.

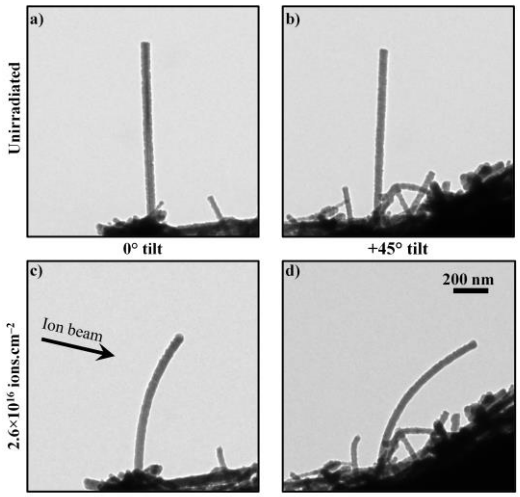

Figure 5: *TEM micrographs of a silicon NW of diameter 50 nm: (a) at 0° x-tilt before*

irradiation; (b) at +45° x-tilt before irradiation; (c) at 0° x-tilt after irradiation; and (d) at +45° x-tilt after irradiation revealing a radius of curvature of 913 nm. After irradiation with 7 keV xenon ions to a fluence of 2.6×10^{16} ions/cm^2, analysis of the bending direction observable at +45° tilt demonstrates that the NW has bent away from the ion beam. The direction of the ion beam during irradiation (projected onto the image plane) is indicated by the arrow in (c) and the scale marker in (d) applies to all four micrographs.

In order to explore the possible mechanisms which could potentially explain the ion-irradiation-induced bending observed in the experiments reported here, consider a typical NW of diameter $2r$ = 50 nm which has undergone a transition from being straight to having a radius of curvature R = 913 nm under irradiation with 7 keV xenon ions to a fluence of 2.6×10^{16} ions/cm^2 as shown in Figure 5. For this NW, σ = 1.028 indicating that the volume on the outside of the radius of curvature was 2.8 % greater relative to the inside volume after irradiation.

3.3 Point defect accumulation and amorphization

Bending was observed to commence immediately upon exposure to the ion beam in the *in-situ* experiments reported here (see video clip S2 in the Supplementary Material). This is consistent with the work of Borschel *et al.* on gallium arsenide [58] and zinc oxide [59] NWs but is notably in contradiction to the work on silicon by Pecora *et al.* where complete amorphization was observed to be necessary to induce bending towards the ion beam [60]. Although the observed immediate response to irradiation rules out complete amorphization as a requirement for ion-beam-induced bending, it is known that amorphous pockets can be induced at the centre of dense atomic-collision cascades [83]. In such a scenario, the amorphous core is surrounded by damaged crystalline material and as irradiation continues the loss of crystallinity progresses by a combination of heterogeneous and homogeneous amorphization. However, at low fluences the probability of a

second ion transiting an amorphous pocket created by a preceding ion is low.

Although there are a range of values in the literature for the volume changes due to the creation of interstitials and vacancies in silicon [46,49,81–85], the cumulative effect of the introduction of these defects ultimately expresses itself as the difference between the densities of crystalline and amorphous silicon. The experimentally measured value of amorphous bulk silicon is 1.8±0.1% less dense than crystalline silicon [89]. Therefore, even under the maximising assumptions that the NW remains in the densest crystalline form on the unirradiated side and is rendered completely amorphous on the irradiated side, simple volume expansion due to the induced damage cannot completely account for the degree of bending shown in Figure 5.

3.4 Separation of vacancy and interstitial distributions

As atomic collision cascades have directionality determined by the trajectory of the instigating particle, the distribution of interstitials is always slightly deeper than that of the vacancies; by definition the interstitials are displaced from the vacancies and those displacements are, on average, along that trajectory. This separation of the two point-defect populations has been put forward by Borschel *et al.* [58] as a possible mechanism as it could cause a contraction in the vacancy-rich shallower region and an expansion in the deeper interstitial-rich region. Based on IDRAGON calculations, the two point-defect distributions have a considerable degree of overlap as shown in Figure 6 for 7 keV xenon ion irradiation of silicon. The total number of atomic displacements, excess vacancies and excess interstitials have been plotted on the same colour scale to give an impression of the relative magnitude of the excesses. As discussed above, modelling work on the volume changes associated with individual point defects in silicon suggests that the distortion due to the slight separation of the defect distributions could occur. However, volume changes per point defect are calculated to be relatively small [46,49,81–85] and given the limited excess defect populations it is not to be expected that this could lead to significant bending. The fact that the shallowest irradiations cause bending away from the ion beam is also inconsistent with the

separation of the vacancy and interstitial distributions being a dominant mechanism. Finally, as demonstrated in the experimental example above, even complete and exclusive amorphization of one half of the NW would be insufficient to induce the observed bending thus casting further doubt on the significance of this separation of the point defect populations being a major driver for bending. However, it cannot be concluded that it will not play some role especially in situations where other driving mechanisms are balanced and where this phenomenon could thus "tip the balance".

Figure 6: *Example of an IDRAGON calculation for 7 keV xenon ion irradiation of a 50 nm silicon NW showing the distributions of atomic displacements, vacancy excess and interstitial excess plotted on the same colour scale.*

3.5 Implantation of ions

The implantation of ions into semiconductor NWs has the potential to induce an expansion; the degree of which being dependant on the ion species and the target material. However, in the open structure of a covalently-bonded semiconductor this can be significantly less than in a close-packed structure such as a metal. As can be seen in table 3, the reversal in bending behaviour occurs in germanium and silicon under irradiation conditions which put the ions in the first half of the NW. For gallium arsenide and zinc oxide the situation is less clear due to the limited data available, but the ranges bracketed by the experimental results also point to a reversal with the implantation peak in the first half. Therefore, it can be concluded that, whilst implantation may play a minor role in

bending the NWs away from the ion beam, beyond a certain depth this effect is dominated by other stronger mechanism(s). Under conditions where $\bar{x}_{ion}/\varnothing > 0.5$, the implantation is again expected to reinforce the resultant deformation as it expands the backside of the NW and assists in the bending towards ion beam. It should be noted that these arguments are based on the assumption that implanted ions remain at the depth at which they come to rest; migration, and especially preferential migration, could alter the outcome.

Electronic energy loss processes can affect volume changes through bond rearrangement which can increase or decrease the rate of amorphization [89]. Nuclear collisions are the dominant energy loss mechanism for ions at low energies while electronic stopping is dominant at higher energies [17,52,90,91]. Under the ion irradiation conditions reported and surveyed here (ion energies $\leq$ 210 keV), the energy loss processes are dominated by nuclear stopping and thus the atomic displacement profiles represent the vast majority of the induced damage. Regardless of $\bar{x}_{disp}$ and $\bar{x}_{ion}$, the greatest electronic energy losses will be close to the irradiated surface where the energy of the incoming ion will be highest and therefore the contribution to bond rearrangement will be greatest in this region. Assuming the electronic energy loss is a driver towards amorphization (i.e. it does not, on average, return bonds towards a crystalline arrangement), then electronic stopping will in all cases be a mechanism for bending away from the ion beam. As bending towards the ion beam is observed at higher energies it can be deduced that electronic energy losses play only a minor role, if any, in the ion energy regime under consideration here.

3.6 Sputtering

Sputtering will remove atoms from the surface of a NW potentially leading to contraction as the surface reconstructs [62]. This will drive NW bending towards the ion beam under all the conditions considered here as none have $\bar{x}_{disp} > 0.55$ whereas a value closer to one would be required for significant sputtering from the back surface which would favour bending away. Therefore, sputtering may reinforce bending towards the ion beam but is dominated by other mechanisms for

the experiments summarised in table 3 where bending is away from the ion beam. Borschel *et al.* [58] have further suggested that sputtering can remove vacancy-rich layers from the irradiated side of a NW at high fluences thus leaving an interstitial-rich layer at the surface in a mechanism which would drive bending away.

3.7 Viscoelastic flow

As viscoelastic flow does not occur in crystalline materials [67], similar arguments apply as those invoked above in consideration of amorphization as a major driving mechanism. The silicon NWs described in reference [92] became amorphous, bent, shortened and broadened during irradiation with 100 keV argon at room temperature to various fluences on the order of ~10^{16} ions/cm^2 and the phenomenon was attributed to surface-tension-driven plastic deformation. Because bending was observed immediately upon the commencement of ion irradiation in the *in-situ* experiments reported here, no significant volume of amorphous material could have been present to allow viscoelastic flow processes, including ion hammering [93], to make a significant contribution. (The ion hammering effect causes a deformation in amorphous materials without a density change via an expansion perpendicular to the ion beam direction and a contraction parallel to the ion beam direction.) However, at higher damage levels it is possible that the role of such a mechanism may increase. This is supported by a paper by Pecora *et al.* [60] which reported that bending of silicon NWs first requires a threshold fluence for amorphization and that bending did not occur if the NW had a crystalline structure.

4. Conclusions

New experiments on the ion-beam-induced bending of semiconductors NWs have been presented alongside a literature review of previous results. Using a custom implementation of the TRIM Monte Carlo computer code, a systematic analysis has been performed to explore the various mechanisms which could potentially drive this deformation. It is concluded that the volumetric

change due to damage accumulation assisted by the proximity of the surface enables shallower irradiations to cause bending away from the ion beam as stress relief at the surface allows the damaged material to expand. For irradiation conditions which cause deeper damage, but importantly still well within the half of the NW nearest the irradiated surface, the bending behaviour is reversed towards the ion beam and it is concluded that sputtering and subsequent surface reconstruction is the only plausible dominant process. Other mechanisms which may play minor roles include the spatial separation between the vacancy and interstitial distributions, swelling caused by implantation, bond rearrangement due to electronic energy loss processes and viscoelastic flow in amorphous material at higher damage levels. Finally, a material-dependent tipping point for the reversal of nanowire bending direction has been found at peak damage depths significantly less than half the nanowire diameter. Further work using computer modelling techniques such as molecular dynamics is now required to test the validity of these deductions and to gain better understanding of the competition between the driving mechanisms which results in tipping points for bending direction at the shallow ion ranges identified in this work.

Acknowledgments

The construction of the MIAMI-1 facility was funded by the Engineering and Physical Sciences Research Council under grant number EP/E017266/1.

References

[1] X. L. Feng, R. He, P. Yang, and M. L. Roukes, "Very high frequency silicon nanowire electromechanical resonators," *Nano Lett.*, **2007**, *7*, 1953–1959.

[2] K. Tomioka, J. Motohisa, S. Hara, K. Hiruma, and T. Fukui, "GaAs/AlGaAs Core Multishell Nanowire-Based Light-Emitting Diodes on Si," *Nano Lett.*, **2010**, *10*, 1639–1644.

[3] B. Tian, X. Zheng, T. J. Kempa, Y. Fang, N. Yu, G. Yu, J. Huang, and C. M. Lieber, "Coaxial silicon nanowires as solar cells and nanoelectronic power sources," *Nature*, **2007**, *449*, 885–889.

[4] Y. Cui, Y. Cui, Z. Zhong, Z. Zhong, D. Wang, D. Wang, W. U. Wang, W. U. Wang, C. M. Lieber, and C. M. Lieber, "High Performance Silicon Nanowire Field Effect Transistors," *Nano Lett.*, **2003**, *3*, 149–152.

[5] J. Xiang, W. Lu, Y. Hu, Y. Wu, H. Yan, and C. M. Lieber, "Ge/Si nanowire heterostructures as high-performance field-effect transistors.," *Nature*, **2006**, *441*, 489–493.

[6] G. Rosaz, B. Salem, N. Pauc, P. Gentile, a Potié, a Solanki, and T. Baron, "High-

performance silicon nanowire field-effect transistor with silicided contacts," *Semicond. Sci. Technol.*, **2011**, *26*, 85020.
[7] Sung Dae Suk *et al.*,"High performance 5nm radius Twin Silicon Nanowire MOSFET (TSNWFET) : fabrication on bulk si wafer, characteristics, and reliability," in *IEEE International Electron Devices Meeting, 2005. IEDM Technical Digest, Washington, DC*, 2005, pp. 717–720.
[8] Z. L. Wang and J. Song, "Piezoelectric nanogenerators based on zinc oxide nanowire arrays.," *Science*, **2006**, *312*, 242–246.
[9] Y. Cui, "Nanowire Nanosensors for Highly Sensitive and Selective Detection of Biological and Chemical Species," *Science*, **2013**, *293*, 1289–1292.
[10] Z. Li, Y. Chen, X. Li, T. I. Kamins, K. Nauka, and R. S. Williams, "Sequence-Specific Label-Free DNA Sensors Based on Silicon Nanowires," *Nano Lett.*, **2004**, *4*, 245–247.
[11] X. Wang, X. Wang, J. Zhou, J. Zhou, J. Song, J. Song, J. Liu, J. Liu, N. Xu, N. Xu, Z. L. Wang and Z. L. Wang, "Piezoelectric field effect transistor and nanoforce sensor based on a single ZnO nanowire.," *Nano Lett.*, **2006**, *6*, 2768–72.
[12] L.-S. Zhong, J.-S. Hu, H.-P. Liang, a.-M. Cao, W.-G. Song, and L.-J. Wan, "Self-Assembled 3D flowerlike iron oxide nanostructures and their application in water treatment," *Adv. Mater.*, **2006**, *18*, 2426–2431.
[13] Z. Fan, D. Wang, P.-C. Chang, W.-Y. Tseng, and J. G. Lu, "ZnO nanowire field-effect transistor and oxygen sensing property[J]," *Appl. Phys. Lett.*, **2004**, *85*, 5923–5925.
[14] Z. L. Wang, "Nanostructures of zinc oxide," *Mater. Today*, **2004**, *7*, 26–33.
[15] M.-J. Caturla, T. Díaz de la Rubia, L. Marqués, and G. Gilmer, "Ion-beam processing of silicon at keV energies: A molecular-dynamics study," *Phys. Rev. B*, **1996**, *54*, 16683–16695.
[16] K. Jun, J. Joo, and J. M. Jacobson, "Focused ion beam-assisted bending of silicon nanowires for complex three dimensional structures," *J. Vac. Sci. Technol. B Microelectron. Nanom. Struct.*, **2009**, *27*, 3043.
[17] Krasheninnikov, A. V. & Banhart, F. Engineering of nanostructured carbon materials with electron or ion beams. *Nat. Mater.* **2007,** 6, 723–733.
[18] R. L. Wallace, Transistor, USA, 2563503, Aug 7, 1951.
[19] T. P. Ma, Paul V. Dressendorf, *Ionizing Radiation Effects in MOS Devices and Circuits*, John Wiley & Sons, 1989.
[20] B. C. Bernard Pajot, *Optical Absorption of Impurities and Defects in Semiconducting Crystals: Electronic Absorption of Deep Centres and Vibrational Spectra*, Springer Science & Business Media, 2012.
[21] R. G. Elliman and J. S. Williams, "Advances in ion beam modification of semiconductors ," *Curr. Opin. Solid State Mater. Sci.*, **2015**, *19*, 49–67.
[22] K. Morita, Y. Inomata, and T. Suemasu, "Optical and electrical properties of semiconducting BaSi2 thin films on Si substrates grown by molecular beam epitaxy," *Thin Solid Films*, **2006**, *508*, 363–366.
[23] N. Bhardwaj and S. Mohapatra, "Ion beam induced evolution of surface morphology and optical properties of SnO_2–ZnO nanocomposite thin films," *Ceram. Int.*, **2015**, *41*, 8614–8622.
[24] P. Rana and R. P. Chauhan, "Ion-beam-induced modifications in the structural and electrical properties of copper oxide selenite nanowires," *Nucl. Instruments Methods Phys. Res. Sect. B Beam Interact. with Mater. Atoms*, **2015**, *349*, 50–55.
[25] M. Piasecki, M. G. Brik, and I. V. Kityk, "Tl_4CdI_6 – Wide band gap semiconductor: First principles modelling of the structural, electronic, optical and elastic properties," *Mater. Chem. Phys.*, **2015**, *163*, 562–568.
[26] X. Guo, S. Momota, N. Nitta, T. Yamaguchi, N. Sato, and H. Tokaji, "Modification of mechanical properties of Si crystal irradiated by Kr-beam," *Appl. Surf. Sci.*, **2015**, *349*, 123–128.
[27] G. Fu, L. Zuo, J. Lian, Y. Wang, J. Chen, J. Longtin, and Z. Xiao, "Ion beam irradiation

effect on thermoelectric properties of Bi2Te3 and Sb2Te3 thin films," *Nucl. Instruments Methods Phys. Res. Sect. B Beam Interact. with Mater. Atoms*, **2015**, *358*, 229–235.
[28] a. G. Hernández, Y. Kudriavtsev, S. Gallardo, M. Avendaño, and R. Asomoza, "Formation of self-organized nano-surfaces on III–V semiconductors by low energy oxygen ion bombardment," *Mater. Sci. Semicond. Process.*, **2015**, *37*, 190–198.
[29] H. K. Nielsen, Capacitance Transient Measurements on Point Defects in Silicon and Silicon Carbide, PhD thesis, Royal Institute of Technology (KTH), Stockholm, Sweeden, 2005.
[30] A. Colli, A. Fasoli, C. Ronning, S. Pisana, S. Piscanec, and A. C. Ferrari, "Ion beam doping of silicon nanowires," *Nano Lett.*, **2008**, *8*, 2188–2193.
[31] C. J. Murphy and N. R. Jana, "Controlling the aspect ratio of inorganic nanorods and nanowires," *Adv. Mater.*, **2002**, *14*, 80–82.
[32] M. S. Gudiksen and C. M. Lieber, "Diameter-selective synthesis of semiconductor nanowires ," *J. Am. Chem. Soc.*, **2000**, *122*, 8801–8802.
[33] X. Duan and C. M. Lieber, "General synthesis of compound semiconductor nanowires," *Adv. Mater.*, **2000**, *12*, 298–302,.
[34] M. S. Gudiksen, L. J. Lauhon, J. Wang, D. C. Smith, and C. M. Lieber, "Growth of nanowire superlattice structures for nanoscale photonics and electronics.," *Nature*, **2002**, *415*, 617–620.
[35] A. Morales and C. Lieber, "A laser ablation method for the synthesis of crystalline semiconductor nanowires," *Science*, **1998**, *279*, 208–211.
[36] S. Reyntjens and R. Puers, "A review of focused ion beam applications in microsystem technology," *J. Micromechanics Microengineering*, **2001**, *11*, 287–300.
[37] D. C. Look, "Recent advances in ZnO materials and devices," *Mater. Sci. Eng. B*, **2001**, *80*, 383–387.
[38] Hong, W. *et al.* Tuning of the Electronic Characteristics of ZnO Nanowire Field Effect Transistors by Proton Irradiation. *ACS Nano*, **2010**, 4, 811–818.
[39] J. Li, D. Stein, C. McMullan, D. Branton, M. J. Aziz, and J. a Golovchenko, "Ion-beam sculpting at nanometre length scales.," *Nature*, **2001**, *412*, 166–169.
[40] L. a. Giannuzzi and F. a. Stevie, "A review of focused ion beam milling techniques for TEM specimen preparation," *Micron*, **1999**, *30*, 197–204.
[41] P. Dai, M. Tan, Y. Y. Wu, L. Ji, L. F. Bian, S. L. Lu, and H. Yang, "Solid-state tellurium doping of AlInP and its application to photovoltaic devices grown by molecular beam epitaxy," *J. Cryst. Growth*, **2015**, *413*, 71–75.
[42] Y. Yamamoto, R. Kurps, J. Murota, and B. Tillack, "Arsenic atomic layer doping in Si using AsH_3," *Solid. State. Electron.*, **2015**, *110*, 29–34.
[43] L. Wang, W. Wang, J. Huang, Y. Zeng, R. Tan, W. Song, and J. Chen, "Argon ion beam assisted magnetron sputtering deposition of boron-doped a-Si:H thin films with improved conductivity," *J. Non. Cryst. Solids*, **2013**, *378*, 177–180.
[44] R. Saive, L. Mueller, E. Mankel, W. Kowalsky, and M. Kroeger, "Doping of TIPS-pentacene via Focused Ion Beam (FIB) exposure," *Org. Electron.*, **2013**, *14*, 1570–1576.
[45] R. Kube, H. Bracht, a. Chroneos, M. Posselt, and B. Schmidt, "Intrinsic and extrinsic diffusion of indium in germanium," *J. Appl. Phys.*, **2009**, *106*, 63534.
[46] M. Tang, L. Colombo, J. Zhu, and T. Diaz de la Rubia, "Intrinsic point defects in crystalline silicon: Tight-binding molecular dynamics studiesof self-diffusion, interstitial-vacancy recombination, and formation volumes," *Phys. Rev. B*, **1997**, *55*, 14279–14289.
[47] R. Lang, a De Menezes, and a Dos Santos, "Ion-Beam-Induced Epitaxial Recrystallization Method and Its Recent Applications," *Cdn.Intechopen.Com*, 1989. [Online]. Available: http://cdn.intechopen.com/pdfs/30910/InTech-Ion_beam_induced_epitaxial_recrystallization_method_and_its_recent_applications.pdf.
[48] E. Rauls and T. Frauenheim, "Entropy of point defects calculated within periodic boundary conditions," *Phys. Rev. B - Condens. Matter. Phys.*, **2004**, *69*, 1–9.
[49] L. Fedina, O. I. Lebedev, G. Van Tendeloo, J. Van Landuyt, O. A. Mironov, and E. H. C. Parker, "In situ HRTEM irradiation study of point-defect clustering in MBE-grown strained

$Si_{1-x}Ge_x$/(001)Si structures," **2000**, *61*, 336–345.
[50] T. Motooka, "The role of defects during amorphization and crystallization processes in ion implanted Si," *Mater. Sci. Eng. A*, **1998**, *253*, 42–49.
[51] J. S. Williams, X. Zhu, M. C. Ridgway, M. J. Conway, B. C. Williams, F. Fortuna, M.-O. Ruault, and H. Bernas, "Preferential amorphization and defect annihilation at nanocavities in silicon during ion irradiation," *Appl. Phys. Lett.*, **2000**, *77*, 4280.
[52] L. Pelaz, L. a. Marqués, and J. Barbolla, "Ion-beam-induced amorphization and recrystallization in silicon," *J. Appl. Phys.*, **2004**, *96*, 5947.
[53] R. D. Goldberg, J. S. Williams, and R. G. Elliman, "Amorphization of silicon by elevated temperature ion irradiation," *Nucl. Instruments Methods Phys. Res. Sect. B Beam Interact. with Mater. Atoms*, **1995**, *106*, 242–247.
[54] C. F. Dee, I. Ahmad, L. Yan, X. Zhou, and B. Y. Majlis, "Amorphization of ZnO nanowires by proton beam irradiation," *Nano*, **2011**, *6*, 259–263.
[55] J. Nord, K. Nordlund, and J. Keinonen, "Amorphization mechanism and defect structures in ion-beam-amorphized Si, Ge, and GaAs," *Phys. Rev. B*, **2002**, *65*, 165329.
[56] A. Colli, A. Fasoli, C. Ronning, S. Pisana, S. Piscanec, and A. C. Ferrari, "Ion beam doping of silicon nanowires," *Nano Lett.*, **2008**, *8*, 2188–2193.
[57] E. Oliviero, S. Peripolli, L. Amaral, P. F. P. Fichtner, M. F. Beaufort, J. F. Barbot, and S. E. Donnelly, "Damage accumulation in neon implanted silicon," *J. Appl. Phys.*, **2006**, *100*, 43505.
[58] C. Borschel, R. Niepelt, S. Geburt, C. Gutsche, I. Regolin, W. Prost, F.-J. Tegude, D. Stichtenoth, D. Schwen, and C. Ronning, "Alignment of semiconductor nanowires using ion beams.," *Small*, **2009**, *5*, 22, 2576–80.
[59] C. Borschel, S. Spindler, D. Lerose, A. Bochmann, S. H. Christiansen, S. Nietzsche, M. Oertel, and C. Ronning, "Permanent bending and alignment of ZnO nanowires.," *Nanotechnology*, **2011**, *22*, 185307.
[60] E. F. Pecora, A. Irrera, and F. Priolo, "Ion beam-induced bending of silicon nanowires," *Phys. E Low-dimensional Syst. Nanostructures*, **2012**, *44*, 1074–1077.
[61] E. F. Pecora, A. Irrera, S. Boninelli, L. Romano, C. Spinella, and F. Priolo, "Nanoscale amorphization, bending and recrystallization in silicon nanowires," *Appl. Phys. A*, **2011**, *102*, 13–19.
[62] N. S. Rajput, Z. Tong, and X. Luo, "Investigation of ion induced bending mechanism for nanostructures," *Mater. Res. Express*, **2014**, *2*, 15002.
[63] L. Romano, N. G. Rudawski, M. R. Holzworth, K. S. Jones, S. G. Choi, and S. T. Picraux, "Nanoscale manipulation of Ge nanowires by ion irradiation," *J. Appl. Phys.*, **2009**, *106*, 114316–6.
[64] Camara, O. *et al.* Effects of temperature on the ion-induced bending of germanium and silicon nanowires. *Mater. Res. Express*, **2017**, 4, 75056.
[65] A. Cui, J. C. Fenton, W. Li, T. H. Shen, Z. Liu, Q. Luo, and C. Gu, "Ion-beam-induced bending of freestanding amorphous nanowires: The importance of the substrate material and charging," *Appl. Phys. Lett.*, **2013**, *102*, 213112–6.
[66] C. Borschel and C. Ronning, "Ion beam irradiation of nanostructures – A 3D Monte Carlo simulation code," *Nucl. Instruments Methods Phys. Res. Sect. B Beam Interact. with Mater. Atoms*, **2011**, *269*, 2133–2138.
[67] H. Trinkaus and a. Ryazanov, "Viscoelastic Model for the Plastic Flow of Amorphous Solids under Energetic Ion Bombardment," *Phys. Rev. Lett.*, **1995**, *74*, 5072–5075.
[68] J. A. Hinks, Van den Berg, and S. E. Donnelly, "MIAMI: Microscope and ion accelerator for materials investigations," *J. Vac. Sci. Technol. A Vacuum, Surfaces, Film.*, **2011**, *29*, 21003–6.
[69] J. F. Ziegler, M. D. Ziegler, and J. P. Biersack, "SRIM – The stopping and range of ions in matter (2010)," *Nucl. Instruments Methods Phys. Res. Sect. B Beam Interact. with Mater. Atoms*, **2010**, *268*, 1818–1823.

[70] R. S. A. D. Schwen, M. Huang, P. Bellon, “The Source Code of the New TRIM Implementation.” [Online]. Available: http://groups.mrl.uiuc.edu/averback/3dtrim/. [Accessed: 01-Mar-2016].
[71] W. Möller, “TRI3DYN - Collisional computer simulation of the dynamic evolution of 3-dimensional nanostructures under ion irradiation,” *Nucl. Instruments Methods Phys. Res. Sect. B Beam Interact. with Mater. Atoms*, **2014**, *322*, 23–33.
[72] Y. G. Li, Y. Yang, M. P. Short, Z. J. Ding, Z. Zeng, and J. Li, “IM3D: A parallel Monte Carlo code for efficient simulations of primary radiation displacements and damage in 3D geometry.,” *Sci. Rep.*, **2015**, *5*, 18130.
[73] F. Schiettekatte, “Fast Monte Carlo for ion beam analysis simulations,” *Nucl. Instruments Methods Phys. Res. Sect. B Beam Interact. with Mater. Atoms*, **2008**, *266*, 1880–1885.
[74] R. E. Stoller, M. B. Toloczko, G. S. Was, A. G. Certain, S. Dwaraknath, and F. A. Garner, “On the use of SRIM for computing radiation damage exposure,” *Nucl. Instruments Methods Phys. Res. Sect. B Beam Interact. with Mater. Atoms*, **2013**, *310*, 75–80.
[75] S. M. Folies, “Comparison of Binary Collision Approximation and Molecular Dynamics for Displacement Cascades in GaAs.” [Online]. Available: http://prod.sandia.gov/techlib/access-control.cgi/2011/118082.pdf. [Accessed: 20-Jan-2016].
[76] E. Holmström, K. Nordlund, and a Kuronen, “Threshold defect production in germanium determined by density functional theory molecular dynamics simulations,” *Phys. Scr.*, **2010**, *81*, 35601.
[77] E. Holmström, a. Kuronen, and K. Nordlund, “Threshold defect production in silicon determined by density functional theory molecular dynamics simulations,” *Phys. Rev. B - Condens. Matter Mater. Phys.*, **2008**, *78*, 1–6.
[78] K. Lorenz, E. Alves, E. Wendler, O. Bilani, W. Wesch, and M. Hayes, “Damage formation and annealing at low temperatures in ion implanted ZnO,” *Appl. Phys. Lett.*, **2005**, *87*, 1–3.
[79] E. Oliviero, S. Peripolli, L. Amaral, P. F. P. Fichtner, M. F. Beaufort, J. F. Barbot, and S. E. Donnelly, "Damage accumulation in neon implanted silicon", *J. Appl. Phys.* **2006,** 100, 43505.
[80] P. D. Edmondson, K. J. Abrams, J. A. Hinks, G. Greaves, C. J. Pawley, I. Hanif, and S. E. Donnelly, "An in situ transmission electron microscopy study of the ion irradiation induced amorphisation of silicon by He and Xe", *Scr. Mater.* **2016,** 113, 190–193.
[81] G. Impellizzeri, S. Mirabella, and M. G. Grimaldi, “Ion implantation damage and crystalline-amorphous transition in Ge,” *Appl. Phys. A Mater. Sci. Process.* **2011,** 103, 323–328.
[82] E. F. Pecora, A. Irrera, and F. Priolo, “Ion beam-induced bending of silicon nanowires,” *Phys. E Low-Dimensional Syst. Nanostructures*, **2012**, *44*, 1074–1077.
[83] P. D. Edmondson, D. J. Riley, R. C. Birtcher, and S. E. Donnelly, “Amorphization of crystalline Si due to heavy and light ion irradiation,” *J. Appl. Phys.*, **2009**, *106*, 43505–43508.
[84] S. A. Centoni, B. Sadigh, G. H. Gilmer, T. J. Lenosky, T. Díaz De La Rubia, and C. B. Musgrave, “First-principles calculation of intrinsic defect formation volumes in silicon,” *Phys. Rev. B - Condens. Matter Mater. Phys.*, **2005**, *72*, 1–9.
[85] S. Öğüt, H. Kim, and J. Chelikowsky, “Ab initio cluster calculations for vacancies in bulk Si,” *Phys. Rev. B*, **1997**, *56*, 11353–11356.
[86] M. J. Aziz, “Pressure and Stress Effects on Diffusion in Si” in Diffusion in Silicon, Trans Tech Publications, vol. 53, 1997.
[87] H. Seong and L. Lewis, “First-principles study of the structure and energetics of neutral divacancies in silicon,” *Phys. Rev. B*, **1996**, *53*, 9791–9796.
[88] A. Antonelli, E. Kaxiras, and D. J. Chadi, “Vacancy in silicon revisited: Structure and pressure effects,” *Phys. Rev. Lett.*, **1998**, *81*, 2088–2091.
[89] J. S. Custer, M. O. Thompson, D. C. Jacobson, J. M. Poate, S. Roorda, W. C. Sinke, and F. Spaepen, “Density of amorphous Si,” *Appl. Phys. Lett.*, **1994**, *64*, 437–439.
[90] Y. Zhang, D. S. Aidhy, T. Varga, S. Moll, P. D. Edmondson, F. Namavar, K. Jin, C. N.

Ostrouchov, and W. J. Weber, “The effect of electronic energy loss on irradiation-induced grain growth in nanocrystalline oxides.,” *Phys. Chem. Chem. Phys.*, **2014**, 16, 8051–8059.
[91] Caturla, M.-J., Díaz de la Rubia, T., Marqués, L. A. & Gilmer, G. H. Ion-beam processing of silicon at keV energies: A molecular-dynamics study. *Phys. Rev. B* **1996,** 54, 16683–16695.
[92] A. Johannes, S. Noack, W. Wesch, M. Glaser, A. Lugstein, and C. Ronning, “Anomalous Plastic Deformation and Sputtering of Ion Irradiated Silicon Nanowires,” *Nano Lett.* **2015,** 15, 3800–3807.
[93] A. Hedler, S. L. Klaumünzer, and W. Wesch, “Amorphous silicon exhibits a glass transition,” *Nat. Mater.*, **2004**, *3*, 804–809.